Continuous Detection of Fluid Leaks into the Body by means of Partially Dissolvable Antennas

Federica Naccarata, *Graduate Student Member, IEEE*, Marco Di Cristofano, and G. Marrocco, *Senior Member, IEEE*

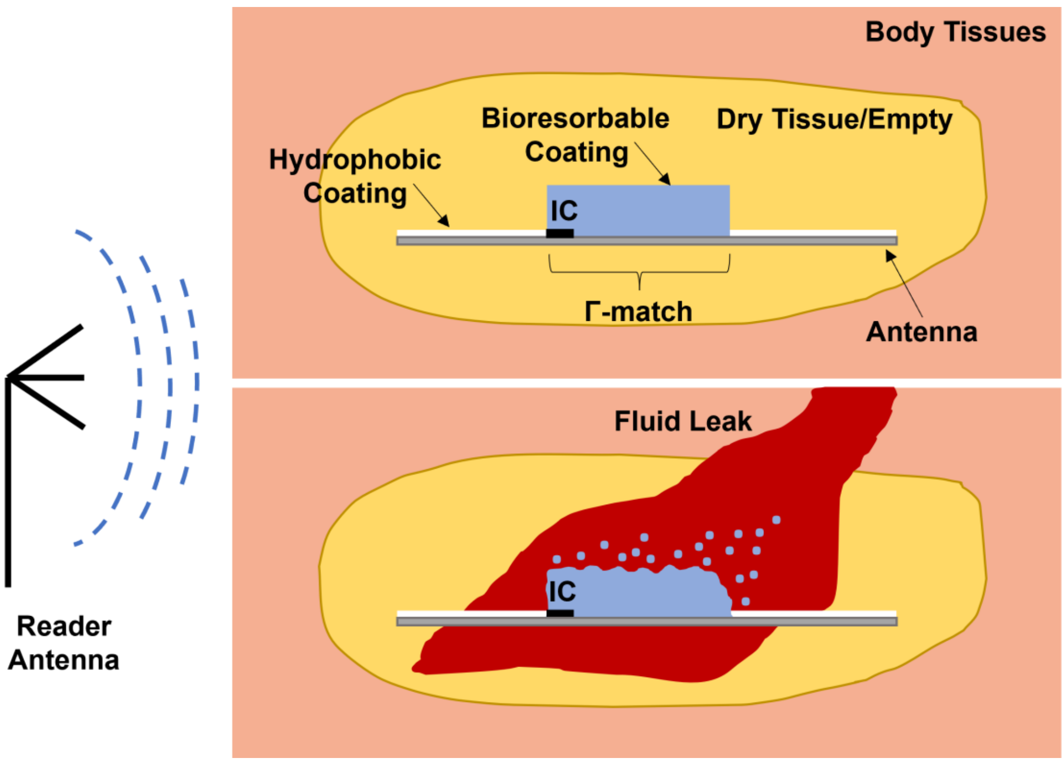

Visual Summary: Concept of a dissolvable-coating-based sensor of fluid leaks in the human body.

Take-Home Messages

- This paper proposes wireless monitoring of fluid leaks into the human body regions exploiting an implanted antenna partially coated by an engineered material and an auto-tuning IC transponder.
- By means of a novel zero-power radiofrequency sensor that exploits dissolvable materials, it is possible to distinguish the degradation by hydrolysis of the bioresorbable coating when in contact with the leaking fluid, with a sensitivity of more 10 units/mm^3.
- The wireless monitoring of endoleaks, after the insertion of a stent graft into the aneurysm sac of an aortic abdominal aneurysm.
- The implanted sensor exploits the *antenna as sensor* paradigm, namely, the impedance of the antenna is modified in a controlled way by the presence of leaks that dissolve a bioresorbable coating. This change is digitalized by an auto-tuning RFID IC and read from outside the body with an external reader antenna.
- The numerical analysis is corroborated by an experimental characterization with a liquid phantom, including electromagnetic measurements to evaluate the robustness of the link and sensor characterization to estimate the achievable dynamic range.

Continuous Detection of Fluid Leaks into the Body by means of Partially Dissolvable Antennas

Federica Naccarata, *Graduate Student Member, IEEE,* Marco Di Cristofano,
Gaetano Marrocco, *Senior Member, IEEE*

***Abstract*—Internal fluid leaks in the human body can be caused by underlying medical disorders. Leakage may also be relevant to implanted stent grafts for the treatment of abdominal aneurysms. Indeed, blood may leak through the stent into the aneurysm sac with the risk of rupture due to increased internal pressure. As standard screenings cannot be performed frequently enough, this paper proposes wireless monitoring of fluid leaks into human body regions exploiting an implanted antenna partially coated by an engineered material and an auto-tuning IC in the UHF RFID band. The presence of fluid modifies the antenna impedance in a controlled way by the hydrolysis of the coating. An indication of this change can be obtained through radiofrequency interrogation from an external reader even when the antenna is implanted at 6 cm. Simulations and tests with a mock-up demonstrated the ability to distinguish the degradation of the bioresorbable coating. The sensor is responsive to up to 3.5 mm^3 of dissolved coating, with a sensitivity of more 10 units/mm^3. Provided that the size of the coating has been properly engineered, the response of the sensor is robust w.r.t. the unpredictable interaction with the fluid.**

***Index Terms*—Implantable Antennas, Bioresorbable, Radio Frequency Identification (RFID), Wireless Monitoring, Battery-Less.**

I. Introduction

Fluid leaks inside the human body [1] can arise as a result of injuries, surgical procedures, infections, or underlying medical conditions. Such fluid leaks can disrupt the normal pressure equilibrium within the body, potentially resulting in hemorrhage and an elevated risk of infection [2] since as they create new pathways for bacteria and other pathogens to enter. Some critical medical conditions include sepsis [3], cerebrospinal fluid (CSF) leaks [4], pleural effusions [5], ascites [6], or endoleaks that may occur following endovascular aortic repair (EVAR) [7]. These conditions can sometimes present subtly and may initially go unnoticed.

Furthermore, leakage can also be associated with vascular implants and in particular, following the insertion of a stent graft, the blood flows outside the stent graft and into the aneurysm sac [8]. These endoleaks can result from various causes, including the detachment of the distal portion of the graft, tears or porosity in the graft material, or retrograde flow from aortic side branches [9]. The immediate consequence is an increase in pressure [7] and, if left untreated, this endotension can cause the enlargement of the sac, with risk of rupture.

The authors are with the Pervasive Electromagnetics Lab, University of Rome Tor Vergata, Via del Politecnico 1, Rome 00133, Italy (e-mail: naccarata@ing.uniroma2.it, gaetano.marrocco@uniroma2.it)

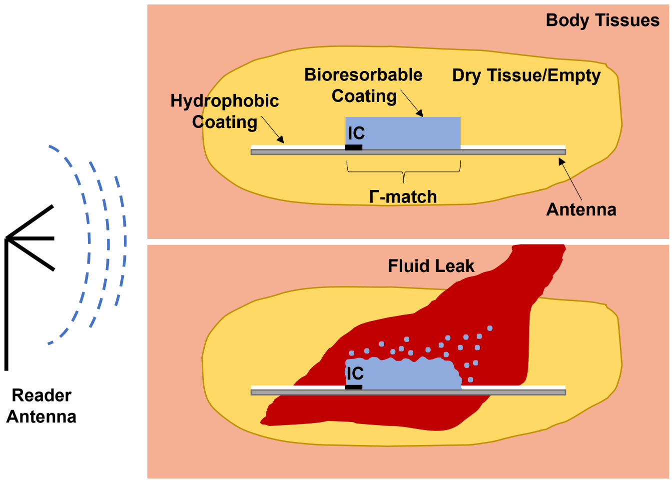

Fig. 1. Concept of dissolvable-coating-based sensor of fluid leaks in the human body.

Currently, postoperative follow-up includes physical examination and imaging screenings such as computed tomography angiography and contrast-enhanced ultrasound [10]. However, these techniques are time consuming and cannot be carried out frequently enough to detect endoleaks in a timely manner due to the harmful doses of radiation and chemical agents.

An alternative diagnostic approach based on in-situ sensors and wireless communication could instead provide a clearer view of the sequence of anticipatory events allowing early diagnosis of endoleaks, thus improving the life expectancy of the patient. Focusing on the cardiovascular domain, the telemetric device in [11] integrated a battery-less blood pressure and the communication with an external interrogator relies on an inductive link. The calibration procedure is invasive and difficult to perform since it requires an angiographic catheter equipped with a pressure sensor [12]. The device has moreover a not negligible size and is kept in place through a metallic basket that could irritate and tear the aneurysm sac. The flexible blood-flow sensor in [13] is instead applied around the vessel, and therefore, it is not suitable for aneurysms. Another solution is based on the modification of a stent implant that is provided with a sensor and whose helicoidal layout is also used as an antenna for bio-telemetry [14]. This idea requires hacking the stent with additional copper wires to interconnect the electronics, making the medical device stiffer. The ultrasonically powered smart stent in [15] includes a voltage-based blood flow sensor and a wireless communication module. A PCB with multiple pressure sensors mounted on the graft can be found in [16]. However, the above devices require several additional elements wrapped around the stent with non-negligible design complexity and a potential change in the mechanical performance of the stent.

This paper proposes a different approach for endoleak detection which can potentially overcome some of the limitations or critical issues of the state of the art, namely *i*) the complexity of the required electronics (which will be reduced to just a single component), *ii*) the need to alter an already assessed and qualified medical device and *iii*) the intrusive and difficult calibration procedure. We resort to the concept of *antenna as sensor*, namely, we will introduce an implanted backscattering antenna whose input parameter, here the impedance, is modified in a controlled way by the presence of leaks so that this change can be read from outside the body. The technological framework is the Radiofrequency Identification (RFID) that, even if originally used for logistics, is now also assessed as a reference technology to achieve sensing capabilities with the smallest electronic complexity as possible, since the antenna itself can become an active part of the transduction mechanism. We will therefore exploit a dissolvable coating to sense the presence of a fluid in the vascular cavity, and the RFID framework for batteryless communication.

RFID technology in the UHF band (860 – 960 MHz) has been already proposed to monitor physiological phenomena inside the human body, especially in combination with implanted prosthesis, thanks to its capability to become an integral part of an existing object. For example, sensing and communication have been added to a medical needle [17] to detect local infection, to a dental implant [18] for temperature monitoring, to a hip prosthesis for the detection of microcrack by means of tattoo-like Space-Filling Curves (SFC) [19]. Cardiovascular applications have been considered as well, such as an augmented stent for wireless restenosis detection [20] and an RFID-enabled aortic valve prosthesis [21], [22] with the capability of temperature monitoring just inside the aortic vessel.

By starting from the preliminary ideas in [23], this paper now proposes an implanted backscattering antenna whose most sensitive part, namely the impedance matching transformer, is coated by a dissolvable substrate which, once in touch with a fluid produced by a leak, will undergo hydrolysis, thus vanishing and changing the local permittivity condition around the antenna. An increasing large portion of the antenna conductor is then exposed to fluid, thus producing a mismatch in the input impedance. This modification will be digitalized locally by means of an auto-tuning RFID IC, which is the only electronic component needed. By calibration, an indication of the presence and severity of the leak can be obtained through radiofrequency interrogation from an external reader (Fig. 1).

The paper is organized as follows. The rationale of sensing by means of a bioresorbable material and an auto-tuning IC is introduced in Section II. Section III describes the numerical analysis for understanding the role of the involved parameters and the evaluation of the wireless link accounting for the mid-field interaction between the sensing element and the external

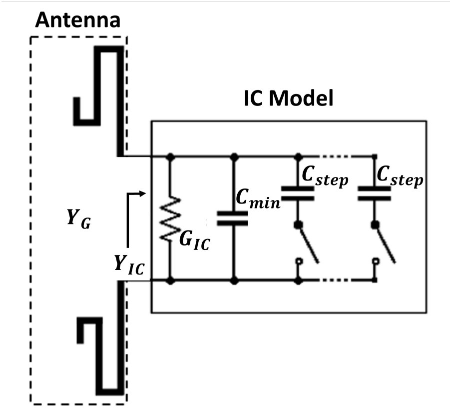

Fig. 2. Equivalent circuit of the auto-tuning IC.

interrogator. Finally, the electromagnetic and sensor performance of a manufactured prototype is resumed in Section IV.

II. Problem Formulation

The sensing of the fluid leak in general, is cast as the monitoring of the onset of the presence of some fluid within a sac that is normally empty or partially filled by a dry tissue. It is reasonable to assume different permittivity and conductivity of the two tissues, with much higher values for the fluid one. Without loss of generalization, and to better fix the sensing rationale, let's hereafter focus on a blood endoleak inside an aneurysm sac following an EVAR intervention. The sac is assumed to be initially filled by dry coagulated blood [24]. The extension to other parts of the body can be considered straightforward. For instance, in the case of endoleak after EVAR, the volumetric measurements in [25] reported an increased aneurysm sac volume (with respect to measurement within 7 days post-implantation) in the range of $[0.2; 241]$ cm^3.

The sensing device (Fig. 1) is here a dipole antenna provided with a $\Gamma-$match impedance transformer, and an auto-tuning RFID IC [26], namely, a particular class of RFID microchip transponders that are capable of dynamically modifying their internal RF impedance to preserve a good impedance matching with the antenna, even in the case of variable boundary conditions [27]. The shape of the antenna can be adapted case by case, depending on the specific application. The antenna is electrically insulated from the body tissues by means of a hydrophobic dielectric coating (insensitive to hydrolysis) except for the central area occupied by the impedance transformer. This region is instead covered by a biocompatible dissolvable material that, when comes in touch with the liquid, will melt by hydrolysis and therefore gradually change the boundary condition over the impedance transformer thus producing a mismatch of the antenna impedance Z_A seen at the Γ-match terminals.

We can expect that the dynamics of the sensor response depends on the interaction between the fluid front and the impedance transformer, as well as on the size and position of the bioresorbable coating. Overall, the endoleak phenomena is complex and should be properly modeled case by case through fluid dynamic simulations that are out of the scope of this paper.

To decouple the electromagnetics phenomena, and hence the design of a wireless sensing device, from the vascular one, we will hereafter refer to an interface quantity, namely the volume of the coating that has been dissolved by the interaction with the leaking fluid. This is a ponderable parameter that will make it possible to master the sensor response to the random interaction with the fluids. Accordingly, denoting with Ψ the amount of the bioresorbable coating that has been dissolved by the hydrolysis, it ultimately generates a variation $\Delta Z_A(\Psi)$. This variation is encoded into digital data by the auto-tuning RFID IC, which automatically changes its internal susceptance. Upon remote interrogation, according to the Gen 2 UHF RFID protocol, it returns an integer number 's', hereafter referred to as *sensor code*, that is proportional to the retuning effort. This quantity is reasonably insensitive to the query modalities. Overall, the following mapping is established:

$$\Psi \rightarrow \Delta Z_A \rightarrow s. \tag{1}$$

The equivalent circuit of the IC can be modeled as a resistor in parallel with a ladder of capacitors (Fig. 2). Therefore, the equivalent RF capacitance of the RFID IC is represented as [28]:

$$C_{IC} = C_{min} + sC_{step} \tag{2}$$

where C_{min} and C_{step} are specific to the particular IC implementation, the IC retuning action is such to minimize the error:

$$|B_{IC}(s) + B_A(\Psi)| \rightarrow 0 \tag{3}$$

where $B_{IC}(s) = 2\pi f C_{IC}(s)$ and $B_A(\Psi)$ are the susceptances of the IC and the antenna, respectively. By combining equation (2) with (3) in the linear range of the device ($S_{min} \leq s \leq S_{max}$), the sensor code returned by the IC is related to the amount dissolved coating Ψ by the equation

$$s(\Psi) = \text{nint}\left\{-\frac{1}{C_{step}}\left[C_{IC}(S_{min}) + \frac{B_A(\Psi)}{2\pi f}\right]\right\} \tag{4}$$

where the operator *'nint'* is a quantization operator that approximates its argument to the nearest integer number. Potential baselines caused by the device manufacturing process and, above all, by implantation variability, can be removed by resorting to a *differential metric* (Δs) [28]:

$$\Delta s(\Psi) = s(0) - s(\Psi) \tag{5}$$

where $s(0)$ is the calibration value when the Γ-match region is still fully protected by the dissolvable coating. The calibration procedure, to be carried out immediately after implantation, is simple and, unlike pressure-based sensors, it is not affected by the external pressure.

By assuming a linear relationship[1] $\Psi \longleftrightarrow \Delta s$, the device sensitivity can be defined as $S(\Psi)=\frac{\Delta s(\Psi_{max})-\Delta s(\Psi_{min})}{\Psi_{max}-\Psi_{min}}$ and is controlled by the size and position of the dissolvable coating.

The sensitivity of the proposed sensor is affected by the dielectric properties of:

1) the transient coating materials and type of fluid involved in the leakage: our sensor exploits the permittivity contrast between the coating and the biological fluid to achieve a sensor outcome. Indeed, when the bioresorbable coating with low permittivity value ($\varepsilon_{HPMC} = 3.2$) is bioresorbed, the local boundary of the Γ-match changes since the coating is replaced by a fluid with high permittivity value ($\varepsilon_{blood} = 61.36$). Therefore, this method can be applied when there is a high permittivity contrast between the bioresorbable coating and the body fluid to be detected, the higher the contrast, the higher the sensitivity of the sensor. Instead, we have verified by simulation that the conductivity of the body fluid has a negligible impact on the sensor response;
2) the surrounding biological material: which affects the communication link (due to a different implantation depth) and the optimal antenna size (that differs if the sensor has been implanted inside a muscle or a fat tissue). The sensor outcomes are instead insensitive to local tissues.

Concerning the selectivity of the sensor, a possible other agent, different than the variation of the local coating, that could modify the sensor code response could be the drift of the auto-tuning module with respect to the body temperature, for instance during fever. This effect is IC-specific and is discussed in Sec. IV-D.

We will hereafter refer to the auto-tuning Axzon Magnus-S3 IC [30] having nominal input admittance $Y_{IC} = 0.482 + j13.5$ *mS* at 900 MHz, with parameters $C_{step} = 1$ pF/512, $C_{min} = 1.9$ pF, conductance $G_{IC} = 0.482$ mS, $S_{min} = 80$, $S_{max} = 400$, and nominal power sensitivity $P_{IC} = -13.6$ dBm.

III. Parametric Analysis

The proposed idea is hereafter evaluated numerically with reference to the simplified body phantom in Fig. 3. It comprises a planar layering of tissues (skin, fat, and muscle, size $236 \times 336 \times 218$ mm^3), a pipe emulating the aorta (length 20 cm, diameter 2 cm) at 7 cm from the skin [31], a metal cylinder emulating the stent (length 5.5 cm, diameter 1.9 cm), and a sphere (diameter 5 cm) that represents the bypassed aneurysm, assumed as filled by coagulated blood, which will be the site of the endoleak. The tissue parameters, at 900 MHz, are derived from [32], while the coagulated blood from [24] (Tab. I). This

[1] In general, the relationship $\Psi \longleftrightarrow \Delta s$ could be even less constrained. Indeed, the useful information relies on a continuous change of Δs w.r.t. an initial condition following the implantation. A monotonic and even linear behavior is, of course, preferred since the progress of the leak could be tracked with more reliability. In the considered configuration, the monotonicity is guaranteed by the Γ-match transformer, which is made by a short-circuit stub whose inductive susceptance changes monotonically by increasing its value when the local permittivity increases [29] due to the degradation of the bioresorbable coating.

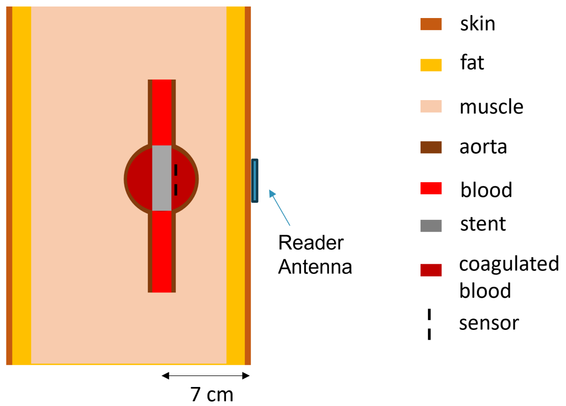

Fig. 3. Reference stratified electromagnetic model of the human abdomen with the sensor inside the aneurysm of the abdominal aorta. The reader antenna is a microstrip slot [33] and applied on the surface of the abdomen.

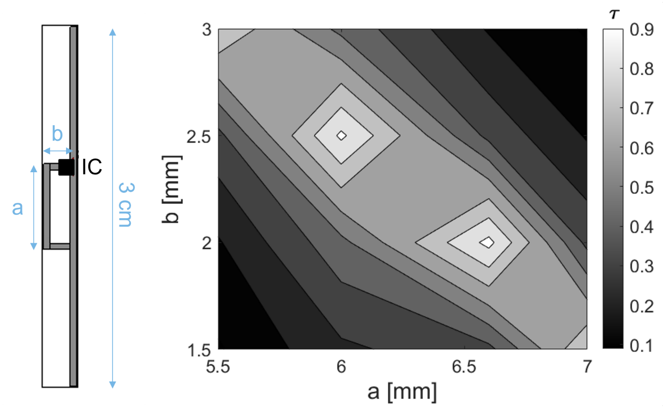

(a) (b)

Fig. 4. (a) Size of the implanted antenna. (b) Isolines of the power transfer coefficient τ at 900 MHz v.s. geometrical parameters of the Γ-match transformer {a, b}.

model can be easily adapted to other cases of endoleaks by changing the shape and electromagnetic parameters of the organs. The specificity of the target object (curvature and material), as for any antenna, is expected to have an impact on the input impedance and hence on the baseline of the sensor code which is, however, removed by the differential measurement.

The reader antenna is the microstrip slot in [33] and is here applied on the skin and properly oriented to couple with the implanted dipole, namely, the slot is orthogonal to the dipole. The dipole is a copper trace (width 0.2 mm, length 3 cm) whose length is similar to the FDA-approved wireless sensor but less thick [12], and is compatible with the size of an abdominal aneurysm. It is placed at a distance of 2 mm from the stent. The antenna and the Γ-match transformer are hosted on a FR4 PCB (thickness 0.8 mm, Fig. 4 (a)) then partly insulated by hydrophobic PolyTetraFluoroEthylene (PTFE) film ($\varepsilon = 2.1$, $tan\delta = 0.00001$ [21], thickness 0.1 mm). The surface of the Γ-match adapter is instead coated by HydroxyPropyl MethylCellulose (HPMC), a semisynthetic polymer used as an external film for the controlled-delivery component in oral medicaments ($\varepsilon = 3.2, \sigma = 0.05$ S/m [34], solubility in water 10 mg/ml [35]). This material has great potential for the biomedical field due to its biocompatibility and low toxicity [36]. We can expect that the dynamics and sensitivity of the sensor response to the interaction with the fluid will also depend on the portion of the impedance transformer which will be globally exposed to the fluid. Accordingly, three possible dissolvable coating configurations are hereafter considered, namely coating of three different sizes (Fig. 5) so that the Γ-match will be fully, half and partially exposed to the fluid. The remaining part will hence be covered by the PTFE insulator.

The electromagnetic response of the implanted antenna is first optimized in transmitting mode, namely neglecting the interrogating device, versus the shape factor of the impedance transformer $\{a,\ b\}$, in the absence of the dissolvable coating, namely when even the sensitive region is covered by PTFE. Simulations are performed by the Finite Element Method by CST Microwave Studio 2023. Fig. 4 (b) shows the isolines of power transfer coefficient τ at 900 MHz versus the parameters $\{a,\ b\}$ of the impedance transformer. To minimize the footprint, the selected configuration is $\{a = 6.6$ mm; $b = 2.0$ mm$\}$ corresponding to $\tau = 0.9$.

A. Communication metrics

The responses of the antenna for variable interactions with the fluid are evaluated in terms of differential sensor code, by Eq. (5), as well as by also quantifying the RFID link. Since the transponder and the interrogating antennas are rather

TABLE I
ELECTRICAL PROPERTIES OF THE TISSUES AT 900 MHZ

	σ	ε_r
Aorta	0.69	44.78
Coagulated Blood	1.15	51.0
Blood	1.54	61.36
Fat	0.05	05.46
Muscle	0.94	55.00
Skin	0.87	41.40

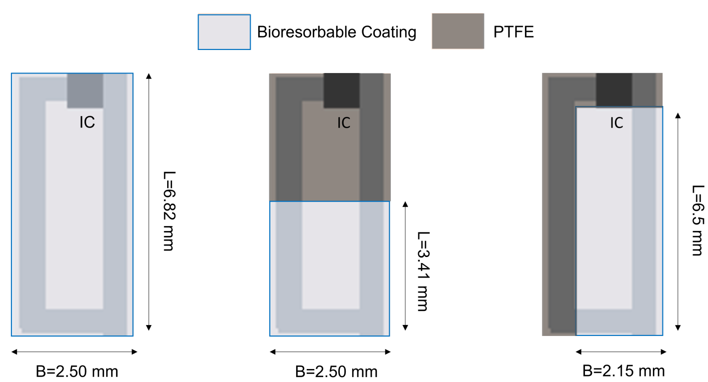

(a) (b) (c)

Fig. 5. Sketch of the three different configurations of bioresorbable coating over the Γ-match impedance adapter: (a) fully covered, (b) half covered, and (c) partially covered.

close to each other, the communication is modeled through a two-port network [37] which is identified by the Admittance Matrix $[Y_{i,j}]$, where port 1 (input) and port 2 (output) refer to the terminals of the reader interrogator and of the implanted device, respectively. The main performance metrics is the Transducer Power Gain G_T, namely the ratio between the power supplied by the reader to the IC ($P_{R\rightarrow T}$) and the power available from the generator ($P_{av,R}$). By exploiting the auto-tuning feature of the IC [22], G_T can be expressed as

$$G_T = \frac{P_{R\rightarrow T}}{P_{av,R}} = \frac{4G_G G_{IC}|Y_{12}|^2}{|(Y_{11}+Y_G)(Y_{22}+Y_{IC}) - Y_{12}^2|^2} \quad (6)$$

where $Y_G = G_G + jB_G$ is the internal admittance of the interrogating antenna and G_{IC} the conductance of the IC. A reliable communication link is established when the following communication margin M(dB) is positive:

$$M = G_T + P_{av,R} - P_{IC} - M_0 \geq 0 \quad (7)$$

where $P_{av,R} = 0$ dB is the maximum power emitted by the reader and $M_0 = 3$ dB is a conservative safe value. By considering as auto-tuning IC the Magnus-S3 by Axzon [30], having nominal power sensitivity $P_{IC} = -13.6$ dBm, the resulting threshold value of G_T to establish the communication is $G_T \geq -40.6$ dB.

B. Electromagnetic models of fluid-antenna interaction

The way the coating will be dissolved by the interaction with the fluid is unpredictable a priori since it is expected to depend on the specific origin of the leak but also on the position of the patient (standing or laying). Hence, some reference fluid-coating interactions will be analyzed next, namely, assuming that the fluid advances toward the antenna in the direction *i*) parallel, *ii*) orthogonal to the extension of the impedance transformer of the antenna, *iii*) as combination of both, namely fully immersed in the fluid, and then *iiii*) along the short side of the Γ-match. The phenomenology of the antenna response is preliminary discussed in details with reference to the coating configuration in Fig. 5 (a) (full cover), so that the whole Γ-match will be exposed to the fluid after the dissolution of the coating. Then, the three configuration of the coating (Fig. 5) are compared with respect to the volume of the dissolved coating.

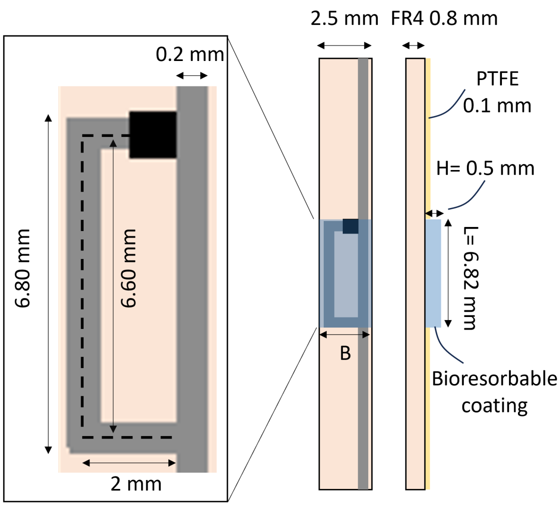

Fig. 6. Representation of the sizes of the antenna, impedance Γ-match transformer, and bioresorbable coating (configuration (a)).

With reference to Fig. 6, the initial sizes of the dissolvable coating are $L = 6.82$ mm, $H = 0.50$ mm and $B = 2.50$ mm that are enough to cover the whole Γ-match (Fig. 5 (a)). The fluid front interactions are emulated by gradually replacing the most external layers of the coating with the fluid by steps of $h = H/10 = 0.05$ mm for orthogonal interaction, $l = L/10 = 0.68$ mm for parallel interaction, and $b = B/10 = 0.25$ mm for interaction along the short side of the Γ-match while keeping the other size fixed. Then, the above orthogonal and parallel interactions are combined (simultaneous thinning L and H).

C. Data Analysis

1) Impact of the fluid front direction: The simulated results are reported in Fig. 7. As hypothesized, the relationship between the variable size of the dissolvable coating and the *differential sensor code* (Fig. 7 (c), (f), (i)) is monotonic, and rather linear w.r.t. the considered change of the geometrical parameters, at least in a portion of the considered range, with an overall variation of the sensor code equal to 60 units. In the case of the orthogonal interaction (Fig. 7 (c)), the device begins to sense the fluid only when $H<0.25$ mm, so that the starting thickness of the coating can be further reduced to roughly one half. If the interaction is instead parallel (Fig. 7 (f)), the response saturates when $L<2$ mm since the IC is not able to compensate for the impedance mismatch of the antenna anymore. By combining the two effects (Fig. 7 (i)), the profile is nearly identical to that of the parallel interaction, which is therefore the dominant one. Instead, when the degradation occurs along the short side of the Γ-match, the device immediately reaches saturation (Fig. 7 (n)).

Concerning the Transducer Power Gain in first three cases (Fig. 7 (b), (e), (h)), in the worst case it degrades below the activation threshold of the IC just when the auto-tuning mechanism would have reached the saturation region. This means that the valuable dynamics of the sensor will be fully captured by the RFID link. Instead, the communication link cannot be established when the degradation occurs along the short side of the Γ-match (Fig. 7 (m)).

2) Impact of the size and position of the dissolvable coating: Finally Fig. 8 summarizes the previous tests with respect to the volume of the dissolvable coating, considering also the other two configurations of the bioresorbable coating (Fig. 5 (b), (c)). The dissolved volume is defined as (in [mm^3])

$$\begin{aligned} V_{dissolved} &= V_{initial} - V_{residual}(n_H, n_L) = \\ &= [H'LB - (H' - n_H h)(L - n_L l)(B - n_B b)] \end{aligned} \quad (8)$$

having considered an initial thickness $H' = H/2 = 0.25$ mm, as discussed above, and $n_{H,L,B} = 1, ..., 10$ being the numbers of removed layers of the coating when simulating

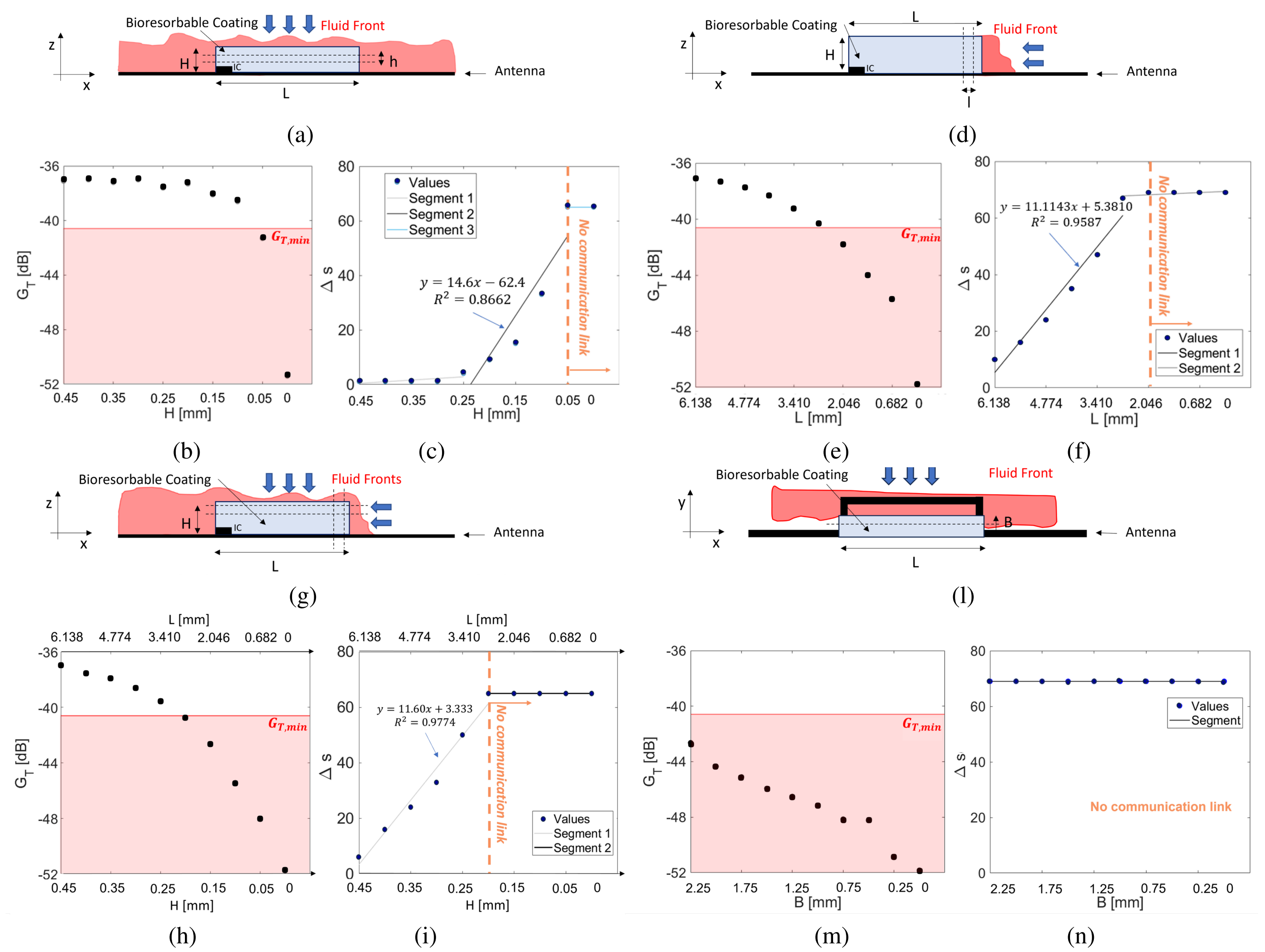

Fig. 7. Numerical analysis of the sensor response for increasing dissolution of the bioresorbable coating occurring along different directions: (a) vertical, (d) horizontal, (g) simultaneous vertical and horizontal, and (l) along the short side of the Γ-match transformer. (b), (e), (h), (m) Transducer Power Gain at 900 MHz, and (c), (f), (i), (n) *differential sensor codes* Δs vs. vertical degradation, horizontal degradation, simultaneous vertical and horizontal degradation, and along the short side of the Γ-match transformer of the bioresorbable coating for each step of degradation.

the fluid front interactions. The distribution of the dataset (Fig. 8 (a)) shows an overall monotonic and quadratic trend before the saturation occurs, except for the degradation along the short side of the Γ-match, so that the sensor can monotonically detect the degradation of the coating for a volume $0.5\ \text{mm}^3 \leq V \leq 3\ \text{mm}^3$ by a 60 units of *differential sensor code* (sensitivity $60/2.5 = 24$ units/mm^3) with an average uncertainty (standard deviation) equal to ± 0.5 mm^3. Considering the other two bioresorbable coating configurations (Fig. 5 (b), (c)), in the case of half-covered impedance adapter (Fig. 8 (b)) the communication link is always guaranteed, since no saturation is reached. However, the sensor outcome during the dissolution along the short side of the Γ-match turns out to be an outlier compared to the other responses, compromising the interpretation of the sensor reading as in the previous case. Finally, the configuration of Fig. 5 (c) guarantees an homogeneous response (Fig. 8 (c)) of the sensor whatever the interaction of the fluid with the coating, although with a decreased sensitivity of approximately $45/3.5 = 13$ units/mm^3, since the overlap area between the metal traces and the coating has been greatly reduced.

Overall, parametric simulations revealed that the response of the sensor can be shaped by properly designing the size of the dissolvable coating and its position w.r.t. the electromagnetically sensitive part of the antenna.

IV. Experimental Corroboration

To corroborate the above numerical analysis, this section introduces a mockup of the implanted device and experimental arrangements for the electromagnetic and sensor characterization.

A. Prototype

The dipole was made of copper trace (width 0.2 mm) etched on a 0.8 mm thick FR4 substrate by a milling machine.

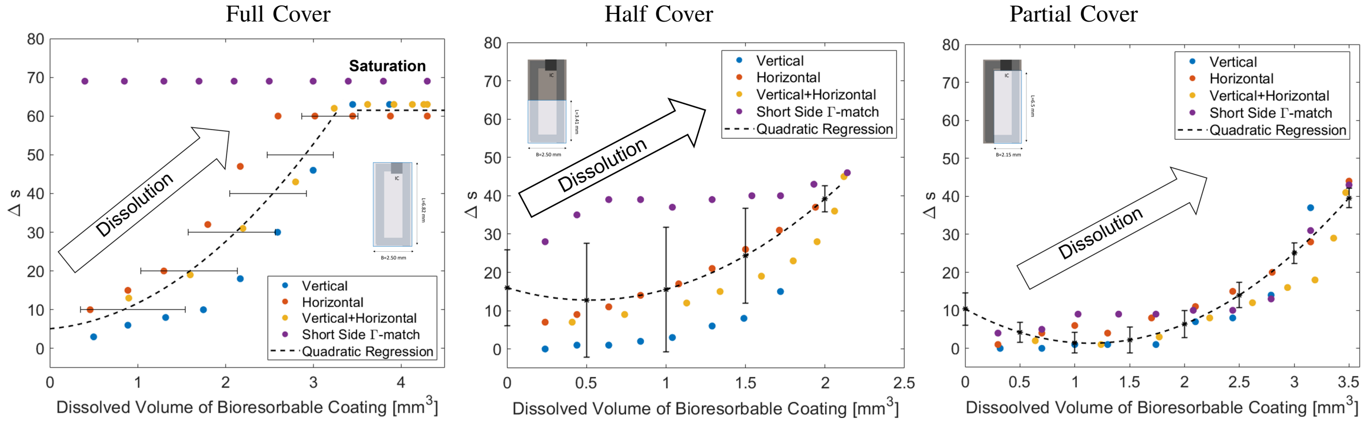

(a) (b) (c)

Fig. 8. *Differential sensor code* Δs vs. the dissolved volume of the bioresorbable coating during the hydrolysis process for a H'=H/2 $= 0.25$ mm thick coating layer with Γ-match transformer: (a) fully covered, (b) half covered, and (c) partially covered. Inset of the bioresorbable coating (Fig. 5) was reproduced.

The prototype was manufactured with common laboratory materials. However, in real applications biocompatibility can be achieved by resorting to silver or gold [38] traces and by coating the FR4 substrate with a biocompatible and antibacterial μm-thick film of Parylene [39]. The IC was mounted on the PCB by means of a solder paste (conductive epoxy CW2400 by Chemtronics, Fig. 9 (a)). Then, the distal parts of the dipole were insulated with PTFE tape (thickness 0.1 mm). The HPMC coating (L = 6.82 mm, H = 0.5 mm) was obtained from commercial oral medicaments and applied on the Γ-match region. The required thickness was achieved by stacking multiple 0.1 mm-thick layers of HPMC that are glue together by some water drops to promote self adhesion and a hot air to weld the layers together (Fig. 9 (a)).

B. Electromagnetic Characterization with a Liquid Phantom

The abdomen was emulated by a PET box ($\varepsilon = 2.1$, $\sigma = 2 \times 10^{-4}$ S/m [21], wall thickness 2 mm) filled with a liquid mixture of water, salt and sugar ($\varepsilon = 54$, $\sigma = 1.05$ S/m [40]), reproducing the lossy human body (Fig. 9 (b)). The device was immersed in the liquid phantom at 6 cm distance from the side wall. The reader antenna was attached to the exterior surface of the container without the silicone layer (since the PET box acts as a spacer itself). The same measurement setup was also simulated to verify the experimental results.

The prototype was electromagnetically characterized in the $750 - 1050$ MHz frequency band by connecting the reader antenna to the Voyantic Tagformance station (Fig. 9 (b)). The measurements lasted less than 30 seconds so that hydrolysis of the remaining coating was not yet activated.

The resulting three measurements of the Transducer Power Gain G_T (Fig. 10) are all above the minimum value required to establish the communication (red line) in the world-wide UHF-RFID band, and compare well with the simulated profile. Fig. 11 shows the measured G_T values when H and L of the dissolvable coating are manually varied as in Sec. III. As expected, the progressive hydrolysis of the HPMC coating monotonically degrades the Transducer Power Gain, but the profiles stay nevertheless above the threshold value for the activation of the RFID link.

C. Sensor Characterization

This further experimental campaign aims to corroborate the achievable dynamic range of the *differential sensor code*. Measurements were carried out using the ThingMagic USB Pro reader (Fig. 9 (c)) that returns the sensor code values.

Fig. 12 shows three measurements of the Δs response in the case of (a) vertical and (b) horizontal degradation of a flat dissolvable coating. Also in this case, the hydrolysis was emulated by manually removing increasing portions of dissolvable coating. Each measurement lasted less than 10 seconds to filter out fluctuations by averaging [28].

Despite an offset, due to manufacturing imperfections and the non-compact structure of the entire coating, the resulting rising trend is monotonic and even more linear than what was predicted.

The last experiments concern the measurement of Δs profile during a real dissolution. Namely, the sensor was immersed in the physiological solution and naturally melted at different times. Each measurement was hence taken continuously to demonstrate that the dissolution time and the overall variation of the sensor codes are proportionally related to the initial thickness of the bioresorbable material. Experiments were repeated with three devices with initial HPMC thicknesses H = $\{0.1, 0.2, 0.3\}$ mm. As discussed in the numerical Section III, the IC is in all cases protected by the PTFE to avoid losing the communication when the sensitive coating (unperturbed length $L = 3.4$ m) completely dissolves (Fig. 13 (a)).

Fig. 13 (b) shows the *differential sensor codes* vs. time during the hydrolysis process. The starting values depend on the amount of HPMC that impacts on the impedance of the Γ-match, while instead, the values at the complete dissolution are comparable (uncertainty of ± 10 sensor code units Fig. 13 (a)). Accordingly, the dissolution times and the overall variation

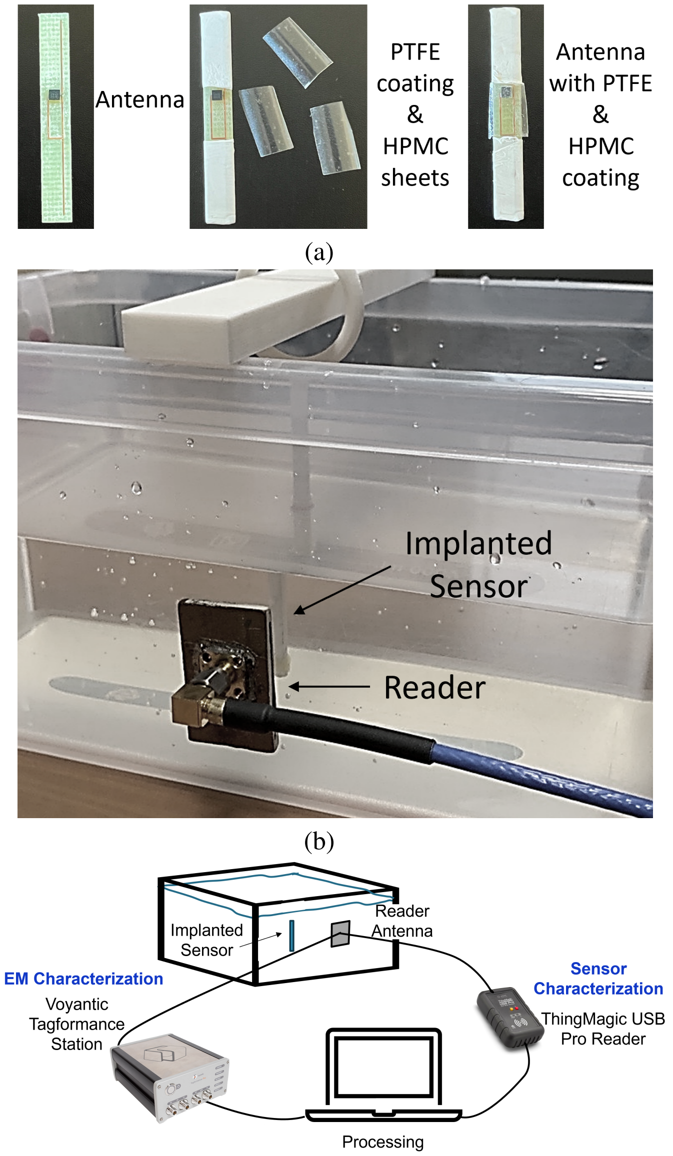

(c)

Fig. 9. Experimental setup involving (a) the implanted prototype immersed into (b) a liquid phantom mimicking the abdomen. (c) Scheme of the measurement setup for electromagnetic and sensor characterization.

of the sensor codes are proportionally related to the initial thickness of the HPMC. Namely, a thicker coating lasts longer and generates larger dynamics. On average, there is a decrease of one unit of sensor code per minute during the dissolution.

D. Impact of the Temperature

Since our human body can experience temperature changes, albeit within a limited range of $5 - 10$ °C, the robustness of the response of the IC equipped with auto-tuning feature was tested at different temperatures. A COTS inlay RFM3200-AER tag by Axzon [41], embedding the same IC used in this work, was placed inside a Binder MKF 56 climatic chamber to perform a test of the returned sensor code when

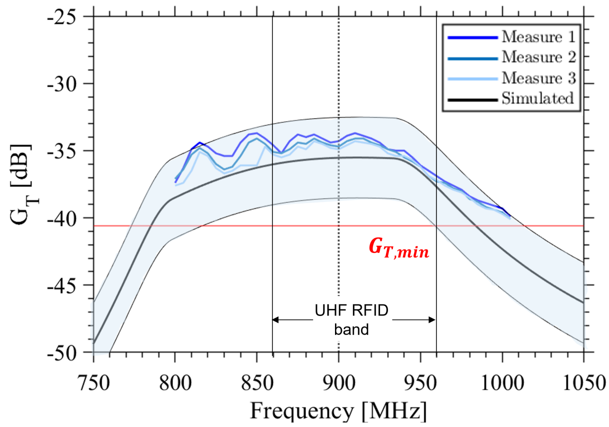

Fig. 10. Simulated and measured Transducer Power Gain G_T vs. frequency of the fully insulated implanted device.

the temperature was raised from 35 °C to 40 °C with humidity set at 50 %. Fig. 14 shows that the *sensor code* is slightly affected by the variation of the temperature with an increment of approximately 1 sensor code/1 °C. Indeed, there is an overall variation of less than 6 sensor codes in average throughout the measure (214 ± 2.7). Since temperature changes within our bodies occur very slowly, the sensor code drift due to the temperature can be corrected in future works with a calibration procedure.

V. Conclusions and Future Prospects

We have introduced a novel zero-power radiofrequency sensor designed for detecting anomalous fluid within the human body. This sensor exploits dissolvable materials. Our simulations and preliminary experiments have illustrated the sensor's potential to distinguish minute degradation of dissolvable coating, on the order of a few mm^3. The most valuable result is that the sensor response can be made homogeneously monotonic with the degradation of the coating regardless of the specific interaction of the fluid, and thus can be considered robust. We can, moreover, adjust the thickness of the dissolvable material to modulate the kinetics of the hydrolysis process as well as to account for scenarios with partially wet boundary conditions. For instance, immediately following the implantation within an aneurysm, there may still be residual liquid blood that will soon coagulate. In such cases, we can design the initial thickness of the sensitive coating to be sufficiently thick (greater than 0.25 mm in the example considered here) to make it insensitive to this remaining liquid that it is drying.

However, while we have introduced the underlying principles of our sensing method, further development of more realistic models is necessary to establish a calibration chart. This chart would provide a relationship between the measured changes in the sensor's code, reflecting the volume of dissolved sensing coating, and the clinical significance of the leak. These measurements could be done periodically or continuously. In the former case, the system is likely to provide binary information, indicating the transition from a dry state to a detected endoleak due to the natural saturation of the sensor.

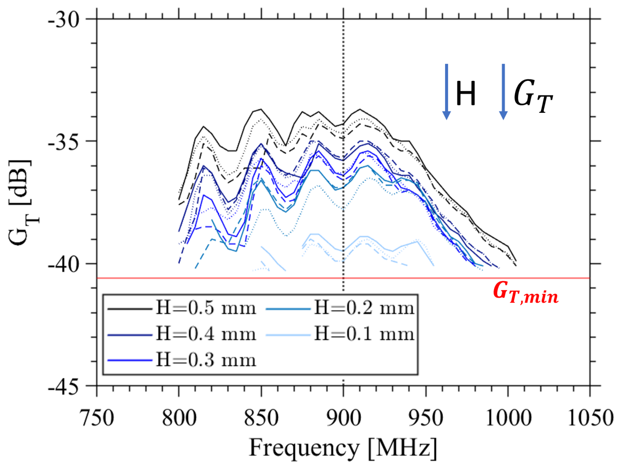

(a)

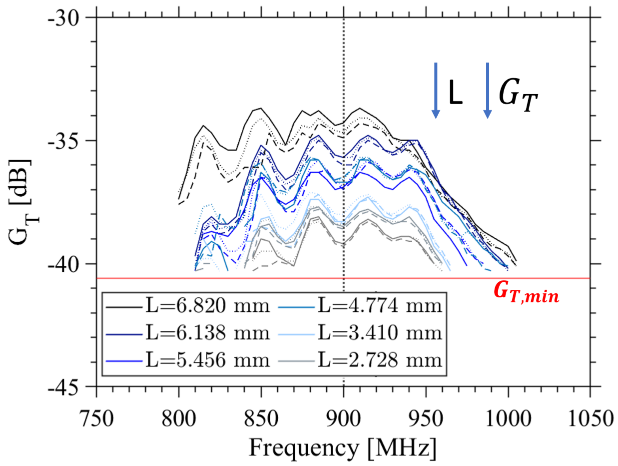

(b)

Fig. 11. Measured Transducer Power Gain G_T vs. frequency in case of: (a) variation of H with constant L, and (b) variation of L with constant H of the bioresorbable coating to emulate the degradation process due to hydrolysis (three measurements of the same color for each case).

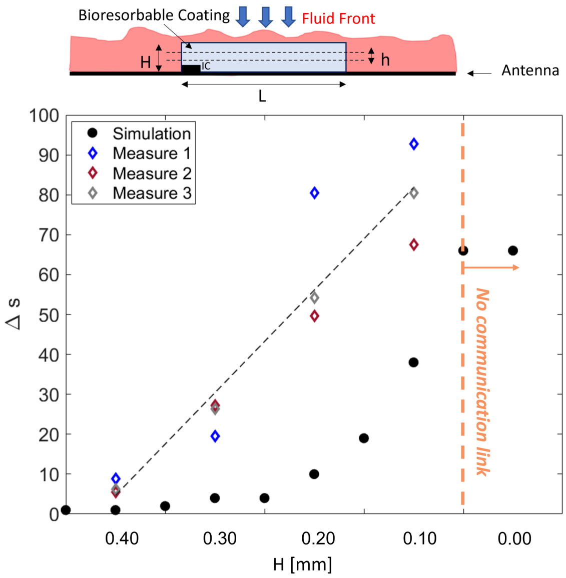

(a)

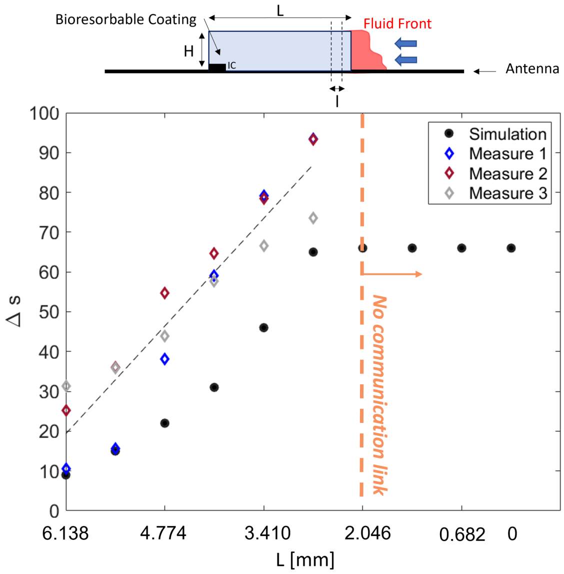

(b)

Fig. 12. Comparison between the *differential sensor code* Δs of the measured and simulated implanted device when: (a) varying the size H (L constant) and (b) varying the size L (H constant) of the bioresorbable coating.

In the latter case, an epidermal reader, affixed to the thorax in the form of a soft plaster [42], could interrogate the implanted sensor at regular intervals, potentially down to minutes or even seconds. This would offer early detection of an endoleak during the immediate post-surgery or rehabilitation phase, even when the patient is outside the hospital, thus prompting more accurate screening.

The resulting sensor is one-time, since the degradation of the coating is irreversible, and hence, it is not reusable. At the first alert of massive leakage, an immediate reintervention is necessary.

However, despite the non-reversible nature of the coating dissolution, the sensor can still provide valuable information by signaling the eventual cessation of liquid blood flow, as it rapidly dries, thus reverting to its initial boundary conditions.

A future advancement of this device could involve making the conductive components of the sensor dissolvable too, thus ensuring their spontaneous disappearance without the need for surgical removal [43] when not necessary anymore.

VI. Acknowledgement

Work partly funded by European Union - NextGenerationEU, ECS 0000024 Rome Technopole, CUP B83C22002820006, PNRR Mission 4, Component 2, Investment 1.5.

References

[1] M.-E. Roumelioti, R. H. Glew, Z. J. Khitan, H. Rondon-Berrios, C. P. Argyropoulos, D. Malhotra, D. S. Raj, E. I. Agaba, M. Rohrscheib, G. H. Murata *et al.*, "Fluid balance concepts in medicine: Principles and practice," *World journal of nephrology*, vol. 7, no. 1, p. 1, 2018.

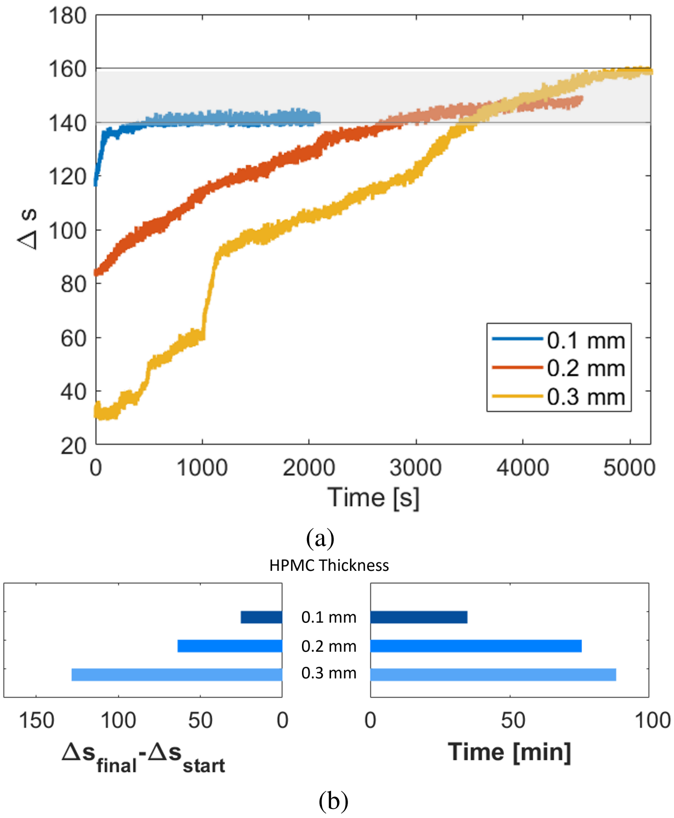

Fig. 13. (a) *Differential sensor code* Δs vs. time of the sensor with different thicknesses of HPMC. The light gray area indicates the zone of uncertainty ± 10. (b) Comparison among *differential sensor code* Δs range and dissolution time for the three thicknesses.

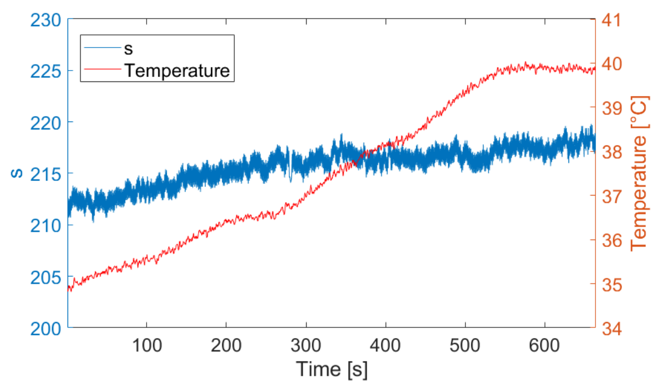

Fig. 14. Example of variation of the *sensor code* due to temperature.

[2] I. H. Chaudry and A. Ayala, "Mechanism of increased susceptibility to infection following hemorrhage," *The American journal of surgery*, vol. 165, no. 2, pp. 59S–67S, 1993.

[3] B. Gyawali, K. Ramakrishna, and A. S. Dhamoon, "Sepsis: The evolution in definition, pathophysiology, and management," *SAGE open medicine*, vol. 7, p. 2050312119835043, 2019.

[4] B. Coucke, L. Van Gerven, S. De Vleeschouwer, F. Van Calenbergh, J. van Loon, and T. Theys, "The incidence of postoperative cerebrospinal fluid leakage after elective cranial surgery: a systematic review," *Neurosurgical review*, pp. 1–19, 2022.

[5] R. W. Light, "Pleural effusions," *Medical clinics*, vol. 95, no. 6, pp. 1055–1070, 2011.

[6] F. D. Gordon, "Ascites," *Clinics in liver disease*, vol. 16, no. 2, pp. 285–299, 2012.

[7] J. Buth *et al.*, "The significance and management of different types of endoleaks," in *Seminars in Vascular Surgery*, vol. 16, no. 2. Elsevier, 2003, pp. 95–102.

[8] L. F. Alexander, C. J. Overfield, D. M. Sella, M. J. Clingan, Y. M. Erben, A. M. Metcalfe, M. L. Robbin, and M. P. Caserta, "Contrast-enhanced us evaluation of endoleaks after endovascular stent repair of abdominal aortic aneurysm," *RadioGraphics*, vol. 42, no. 6, pp. 1758–1775, 2022.

[9] J. Buth, P. L. Harris, C. van Marrewijk, and G. Fransen, "The significance and management of different types of endoleaks," in *Seminars in Vascular Surgery*, vol. 16, no. 2. Elsevier, 2003, pp. 95–102.

[10] G. I. Karaolanis, C. N. Antonopoulos, E. Georgakarakos, G. D. Lianos, M. Mitsis, G. K. Glantzounis, A. Giannoukas, and G. Kouvelos, "Colour duplex and/or contrast-enhanced ultrasound compared with computed tomography angiography for endoleak detection after endovascular abdominal aortic aneurysm repair: a systematic review and meta-analysis," *Journal of Clinical Medicine*, vol. 11, no. 13, p. 3628, 2022.

[11] M. Veletic, E. H. Apu, M. Simic, J. Bergsland, I. Balasingham, C. H. Contag, and N. Ashammakhi, "Implants with sensing capabilities," *Chemical Reviews*, vol. 122, no. 21, pp. 16 329–16 363, 2022.

[12] T. Ohki, K. Ouriel, P. G. Silveira, B. Katzen, R. White, F. Criado, and E. Diethrich, "Initial results of wireless pressure sensing for endovascular aneurysm repair: the APEX Trial-Acute pressure measurement to confirm aneurysm sac exclusion," *Journal of vascular surgery*, vol. 45, no. 2, pp. 236–242, 2007.

[13] Y. Hacohen and S. J. A. Majerus, "A flexible double helix inductive antenna for rfid vascular flow sensing," *IEEE Sensors Journal*, vol. 23, no. 17, pp. 19 044–19 051, 2023.

[14] S. A. A. Shah, Y.-H. Lim, and H. Yoo, "A novel development of endovascular aortic stent system featuring promising antenna characteristics," *IEEE Transactions on Antennas and Propagation*, vol. 70, no. 3, pp. 2214–2222, 2021.

[15] S. Islam, X. Song, E. T. Choi, J. Kim, H. Liu, and A. Kim, "In vitro study on smart stent for autonomous post-endovascular aneurysm repair surveillance," *IEEE Access*, vol. 8, pp. 96 340–96 346, 2020.

[16] B. John, C. Spink, M. Braunschweig, R. Ranjan, D. Schroeder, A. Koops, G. Woldt, I. Rauh, A. Leuzinger, G. Adam *et al.*, "Telemetric system for monitoring of endoleak in abdominal aorta aneurysm using multiple pressure sensors integrated on a stent graft," in *2016 IEEE Biomedical Circuits and Systems Conference (BioCAS)*. IEEE, 2016, pp. 384–387.

[17] F. Naccarata, N. Panunzio, M. D. Cristofano, G. Tufi, F. Ciafrei, M. Cinelli, F. D. Fave, C. Magnante, and G. Marrocco, "Semi-implantable antenna integrated into a medical needle," in *2023 17th European Conference on Antennas and Propagation (EuCAP)*, 2023, pp. 1–4.

[18] N. Panunzio *et al.*, "Cyber-tooth: antennified dental implant for RFID wireless temperature monitoring," in *2021 IEEE International Conference on RFID Technology and Applications (RFID-TA)*. IEEE, 2021, pp. 211–214.

[19] S. Nappi, L. Gargale, F. Naccarata, P. P. Valentini, and G. Marrocco, "A fractal-RFID based sensing tattoo for the early detection of cracks in implanted metal prostheses," *IEEE Journal of Electromagnetics, RF and Microwaves in Medicine and Biology*, vol. 6, no. 1, pp. 29–40, 2022.

[20] C. Occhiuzzi, G. Contri, and G. Marrocco, "Design of implanted RFID tags for passive sensing of human body: the STENTag," *IEEE Transactions on Antennas and Propagation*, vol. 60, no. 7, pp. 3146–3154, 2012.

[21] F. Naccarata, C. Occhiuzzi, R. Verzicco, and G. Marrocco, "Wireless and zero-power trans-cardiac link with antennified aortic valve bioprostheses," *IEEE Journal of Electromagnetics, RF and Microwaves in Medicine and Biology*, vol. 7, no. 1, pp. 15–23, 2022.

[22] F. Naccarata and G. Marrocco, "Integrated wireless RFID temperature sensor for biological aortic valve prostheses," *IEEE Journal of Radio Frequency Identification*, pp. 1–1, 2023.

[23] F. Naccarata, M. Di Cristofano, , and G. Marrocco, "RFID-based endoleak detection by dissolvable antennas and auto-tuning ic," in *2023 IEEE 13th International Conference on RFID Technology and Applications (RFID-TA)*, 2023.

[24] A. Santorelli, S. Fitzgerald, A. Douglas, K. Doyle, and M. OâHalloran, "Dielectric profile of blood clots to inform ischemic stroke treatments," in *2020 42nd Annual International Conference of the IEEE Engineering in Medicine & Biology Society (EMBC)*. IEEE, 2020, pp. 3723–3726.

[25] M. Schnitzbauer, O. Güntner, W. A. Wohlgemuth, F. Zeman, M. Haimerl, C. Stroszczynski, and R. Müller-Wille, "Ct after endovascular repair of abdominal aortic aneurysms: diagnostic accuracy of diameter mea-

surements for the detection of aneurysm sac enlargement," *Journal of Vascular and Interventional Radiology*, vol. 29, no. 2, pp. 178–187, 2018.
[26] G. M. Bianco, S. Amendola, and G. Marrocco, "Near-field constrained design for self-tuning uhf-rfid antennas," *IEEE Transactions on Antennas and Propagation*, vol. 68, no. 10, pp. 6906–6911, 2020.
[27] M. C. Caccami and G. Marrocco, "Electromagnetic modeling of self-tuning rfid sensor antennas in linear and nonlinear regimes," *IEEE Transactions on Antennas and Propagation*, vol. 66, no. 6, pp. 2779–2787, 2018.
[28] F. Naccarata, G. M. Bianco, and G. Marrocco, "Sensing performance of multi-channel RFID-based finger augmentation devices for Tactile Internet," *IEEE Journal of Radio Frequency Identification*, 2022.
[29] H. Tolles, "How to design gamma-matching networks," *Ham. Radio*, pp. 46–55, 1973.
[30] Axzon, RRFM3300-E Magnus-S3 M3E passive sensor IC, available on line. Accessed: May 2, 2023. [Online]. Available: https://axzon.com/rfm3300-e-magnus-s3-m3e-passive-sensor-ic/
[31] M. R. Skilton, D. S. Celermajer, E. Cosmi, F. Crispi, S. S. Gidding, O. T. Raitakari, and E. M. Urbina, "Natural history of atherosclerosis and abdominal aortic intima-media thickness: rationale, evidence, and best practice for detection of atherosclerosis in the young," *Journal of Clinical Medicine*, vol. 8, no. 8, p. 1201, 2019.
[32] IFAC-CNR., "Calculation of the dielectric properties of body tissues in the frequency range 10 Hz - 100 GHz," available on line. Accessed: Oct. 1, 2023. [Online]. Available: http://niremf.ifac.cnr.it/
[33] C. Miozzi, G. Saggio, E. Gruppioni, and G. Marrocco, "Constrained safety-integrity performance of through-the-arms uhf-rfid transcutaneous wireless communication for the control of prostheses," *IEEE Journal of Radio Frequency Identification*, vol. 3, no. 4, pp. 236–244, 2019.
[34] A. A. Barba, A. Dalmoro, and M. d'Amore, "Microwave assisted drying of cellulose derivative (HPMC) granular solids," *Powder technology*, vol. 237, pp. 581–585, 2013.
[35] Sigma Aldrich HPMC, accessed: Dec. 2, 2023. [Online]. Available: https://www.sigmaaldrich.com/IT/it/product/sigma/h7509
[36] K. Deshmukh, M. B. Ahamed, R. Deshmukh, S. K. Pasha, P. Bhagat, and K. Chidambaram, "Biopolymer composites with high dielectric performance: interface engineering," in *Biopolymer composites in electronics*. Elsevier, 2017, pp. 27–128.
[37] S. J. Orfanidis, *Electromagnetic Waves and Antennas*. [Online]. Available: http://eceweb1.rutgers.edu/ orfanidi/ewa/
[38] N. Manam, W. Harun, D. Shri, S. Ghani, T. Kurniawan, M. H. Ismail, and M. Ibrahim, "Study of corrosion in biocompatible metals for implants: A review," *Journal of alloys and compounds*, vol. 701, pp. 698–715, 2017.
[39] M. Golda-Cepa, K. Engvall, M. Hakkarainen, and A. Kotarba, "Recent progress on parylene c polymer for biomedical applications: A review," *Progress in Organic Coatings*, vol. 140, p. 105493, 2020.
[40] Speag Swiss, accessed: Oct. 2, 2023. [Online]. Available: https://speag.swiss/components/materials-liquids/msl/
[41] Axzon RFM3200 Wireless Flexible Temperature Sensor, available on line. Accessed: May 2, 2023. [Online]. Available: https://axzon.com/rfm3200-wireless-flexible-temperaturesensor/
[42] F. Camera, C. Miozzi, F. Amato, C. Occhiuzzi, and G. Marrocco, "Experimental assessment of wireless monitoring of axilla temperature by means of epidermal battery-less RFID sensors," *IEEE Sensors Letters*, vol. 4, no. 11, pp. 1–4, 2020.
[43] Q. Zhang, Q. Liang, and J. A. Rogers, "Water-soluble energy harvester as a promising power solution for temporary electronic implants," *APL Materials*, vol. 8, no. 12, 2020.

Federica Naccarata (Graduate Student Member, IEEE) received the M.Sc. (Hons.) degree in Medical Engineering from the University of Rome Tor Vergata, Rome, Italy in 2021. She is currently pursuing a Ph.D. degree in Computer Science, Control and Geoinformation within the Pervasive Electromagnetics Lab at the University of Rome Tor Vergata, and she is a part-time R&D Medical Engineer at RADIO6ENSE Srl. Her research interests mainly include RFID systems, implantable antennas, and sensors. She won the Gaetano Latmiral Award at the XXIV Riunione Nazionale di Elettromagnetismo (RiNEm) 2022 and the Best Paper Award (2nd prize - regular papers) at the 2023 IEEE International Conference on RFID Technology and Applications (RFID-TA).

Marco Di Cristofano received the M.Sc. degree (Hons.) in Medical Engineering from the University of Rome Tor Vergata, Italy, in 2023. He is currently pursuing a Ph.D. degree in Information and Communications Technologies (ICT) at Sapienza University, Rome, Italy. His research topic is based on the development of quality assurance (QA) protocols for oncological hyperthermia systems. He won the Best Paper Award (2nd prize - regular papers) at the 2023 IEEE International Conference on RFID Technology and Applications (RFID-TA).

Gaetano Marrocco (Senior Member, IEEE) is Full Professor of Electromagnetics Engineering at the University of Roma Tor Vergata, where he currently leads the Medical Engineering School. Since 2002, he has been a pioneer in Radiofrequency Identification and Sensing. His current research focuses on wireless-activated sensors, Wearable and Epidermal Electronics, and structural antennas for sensorized skins, smart prostheses, and finger augmentation devices for Tactile Internet. He serves as an Associate Editor of the IEEE Journal of Radiofrequency Identification and the IEEE Journal of Flexible Electronics. Additionally, he chairs the Italian Section of URSI Commission D Electronics and Photonics and is a co-founder and president of the University spin-off RADIO6ENSE. RADIO6ENSE is actively involved in short-range electromagnetic sensing for Industrial Internet of Things, Smart Manufacturing, Automotive, and Digital Health. He is also listed in the PLOS 2022 ranking of the Top 2% Scientists Worldwide.